parison with those of theoretical approaches. A calculated value of the heat of formation of **1** (169 kcal mol^{-1}) has been reported without specifying its most stable conformation.[20] Very recently, MINDO/3 and MNDO calculations concerning the boat and chair conformations of **1** and the transition states of 1-2, 1-3, and 1-4 hydride shifts have been published. A "facile" **1** → **2** rearrangement has been noted in the course of the calculations, consistent with the evidence presented in this study, but unfortunately the specific reaction pathway has not been studied in detail.[1b]

Acknowledgment. This work has been financially supported by the Italian National Research Council (CNR). The skillful assistance of A. Di Marzio and F. Porretta is gratefully acknowledged.

Registry No. MeOH, 67-56-1; 1,4-C_4H_8Br, 110-52-1; cyclohexylium, 22499-63-4; cyclohexane-t_2, 84142-46-1; cyclohexene, 110-83-8.

(20) Jorgensen, W. L., quoted in: Harris, J. M.; Shafer, S. Y. *J. Comput. Chem.* **1982**, *3*, 208.

Optical Activity of Monoolefins: RPA Calculations and Extraction of the Mechanisms in Kirkwood's Theory. Application to (−)-*trans*-Cyclooctene and (3*R*)-3-Methylcyclopentene

Aage E. Hansen*[1a] and Thomas D. Bouman*[1b]

Contribution from the Department of Chemistry, Southern Illinois University at Edwardsville, Edwardsville, Illinois 62026, and the Department of Physical Chemistry, H. C. Ørsted Institute, Universitetsparken 5 DK-2100 Copenhagen Ø, Denmark. *Received January 21, 1985*

Abstract: We present ab initio extended basis set calculations of the electronic (UV and CD) spectra of (−)-*trans*-cyclooctene and (3*R*)-3-methylcyclopentene in the random phase approximation (RPA). The nature of the excitations is discussed by means of approximate improved virtual orbitals (IVO's), transition densities, and charge rearrangement densities, and we use spectrum simulations to assist the comparison with experimental results. When a basis of localized molecular orbitals is used and effective bond transition moments are introduced, the RPA expression for the rotatory strength is cast in a form isomorphic with Kirkwood's original theory of optical rotatory power, and we present the resulting analysis of the chiroptical properties of the title compounds. To assist this analysis and to establish connection to previous work, we include calculations on ethylene and *trans*-2-butene, distorted as in (−)-*trans*-cyclooctene. Our computed results for ethylene and the other title molecules give a very satisfactory account of olefin spectra, for both valence and Rydberg excitations. The IVO contour plots of the $\pi \rightarrow$ 3p Rydberg excitations show that the effective quantization axes of the 3p IVO's are governed by the gross shape of the molecule as opposed to the local symmetry of the chromophore. The Kirkwood analysis shows that the mechanisms for the chiroptical properties of the title compounds are quite different.

I. Introduction

Over the years, the electronic spectra and the circular dichroism (CD) of monoolefins have been studied theoretically and experimentally from two different points of view. One perspective is the elucidation of the electronic properties of the ethylenic double bond, through the study of the combined effects of low-symmetry and restricted-motion molecular environments on the spectra. This viewpoint is exemplified by spectroscopic studies[2,3] and by electron impact[4] and photoelectron studies.[5] For the chiral molecules studied in ref 2 and 3, one gains in addition that the selection rules and intensity distributions in CD are quite different from those of ordinary absorption spectra.[6,7] The other perspective is to use the ethylenic chromophore as a structural probe, motivated largely by the success of the octant rule[7] for carbonyl compounds. This approach is represented by a number of studies combining experimental data and theoretical models in an attempt to generate rules for structure–CD correlations in rigid monoolefins.[8-15] Of course, the two approaches are closely related since meaningful structure correlations presuppose secure spectral assignments.

Ethylene itself has been a computational favorite since the dawn of quantum chemistry (for leading references, see ref 16–18), whereas ab initio calculations on larger monoolefins are quite sparse.[19] Among chiral monoolefins, attention has been focused on two systems, namely (3*R*)-3-methylcyclopentene (Figure 1), whose low-lying excitations were treated recently by an ab initio SCF method,[20] and (−)-*trans*-cyclooctene (Figure 2), whose $\pi \rightarrow \pi^*$ excitation has been studied by semiempirical[21] and minimal basis set ab initio methods[22] and for which twisted butene[23,24] and

(1) (a) H. C. Ørsted Institute. (b) Southern Illinois University.
(2) Gross, K. P.; Schnepp, O. *Chem. Phys. Lett.* **1975**, *36*, 531.
(3) Mason, M. G.; Schnepp, O. *J. Chem. Phys.* **1973**, *59*, 1092.
(4) Johnson, K. E.; Johnston, D. B.; Lipsky, S. *J. Chem. Phys.* **1979**, *70*, 3844.
(5) Mintz, D. M.; Kuppermann, A. *J. Chem. Phys.* **1979**, *71*, 3499.
(6) Schellman, J. A. *Chem. Rev.* **1975**, *75*, 323.
(7) Hansen, Aa. E.; Bouman, T. D. *Adv. Chem. Phys.* **1980**, *44*, 545.
(8) Anderson, N. H.; Costin, R. C.; Shaw, J. R. *J. Am. Chem. Soc.* **1974**, *96*, 3692.
(9) Drake, A. F.; Mason, S. F. *Chem. Commun.* **1973**, 253.
(10) Drake, A. F.; Mason, S. F. *Tetrahedron* **1977**, *33*, 937.
(11) Gawroński, J. K. *Tetrahedron* **1977**, *33*, 1235.
(12) Hudec, J.; Kirk, D. N. *Tetrahedron* **1976**, *32*, 2475.
(13) Weigang, O. E. *J. Am. Chem. Soc.* **1979**, *101*, 1965.
(14) Scott, A. I.; Wrixon, A. D. *Tetrahedron* **1970**, *26*, 3695.
(15) Scott, A. I.; Yeh, C. Y. *J. Chem. Soc., Faraday Trans. 2* **1975**, *71*, 447.
(16) Merer, A. J.; Mulliken, R. S. *Chem. Rev.* **1969**, *69*, 639.
(17) Petrongolo, C.; Buenker, R. J.; Peyerimhoff, S. D. *J. Chem. Phys.* **1982**, *76*, 3655.
(18) Nakatsuji, K. *J. Chem. Phys.* **1984**, *80*, 3703.
(19) Bonačič-Koutecký, V.; Pogliani, L.; Persico, M.; Koutecký, J. *Tetrahedron* **1982**, *38*, 741.
(20) Levi, M.; Cohen, D.; Schurig, V.; Bach, H.; Gedanken, A. *J. Am. Chem. Soc.* **1980**, *102*, 6972.
(21) Levin, C. C.; Hoffmann, R. *J. Am. Chem. Soc.* **1972**, *94*, 3446.
(22) Rauk, A.; Barriel, J. M.; Ziegler, T. *Prog. Theor. Org. Chem.* **1977**, *2*, 467.

0002-7863/85/1507-4828$01.50/0

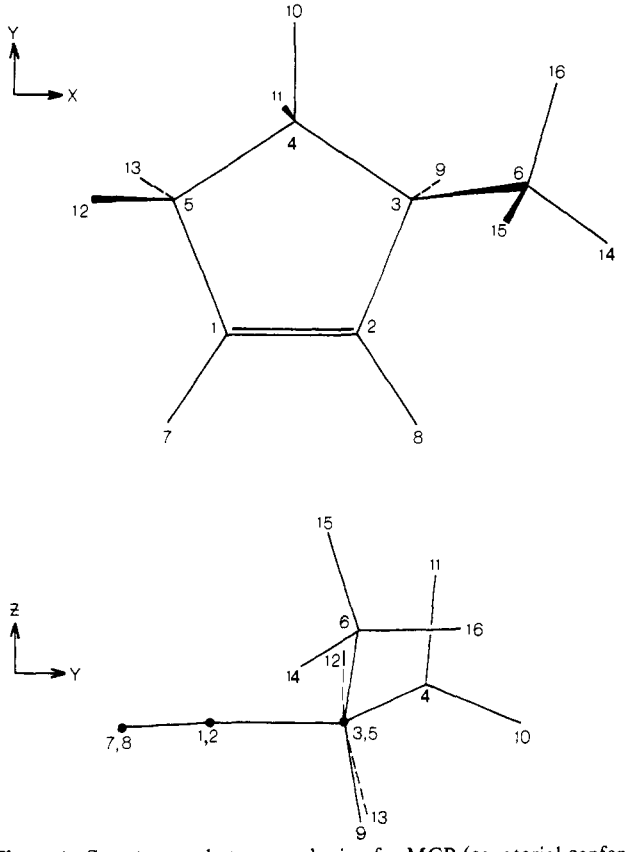

Figure 1. Structure and atom numbering for MCP (equatorial conformation).

ethylene[23-30] have been used quite extensively as models. In an alternative approach, Scott and Yeh[15] demonstrated that a large part of the optical rotatory power of (−)-*trans*-cyclooctene could be accounted for in a polarizability theory approach.

trans-Cyclooctene (TCO) and methylcyclopentene (MCP) are in fact well suited for computational studies. Their experimental chiroptical spectra are available,[3,20] their size allows quite elaborate calculations, and they exemplify two characteristic chiroptical models,[7] namely an inherently dissymmetric chromophore (TCO) and a dissymmetrically perturbed, planar chromophore (MCP). This invites calculation and analysis of both molecules by a single method, and we shall present the results of such an approach here. Included in this treatment are calculations on the fragment molecules ethylene and *trans*-2-butene distorted as in TCO; this also establishes the connection to previous work. The computational framework we shall use is the ab initio random phase approximation (RPA),[7,30-32] using extended basis sets to account for Rydberg as well as valence excitations. The computational details are given in section IV, which also contains an overview of the results in the form of correlation diagrams.

Our main emphasis will be on analyzing the results of the excitations and the mechanisms for the chiroptical intensities. The excitation analyses (i.e., the spectral assignments) are done in terms of transition and rearrangement densities and by the study of

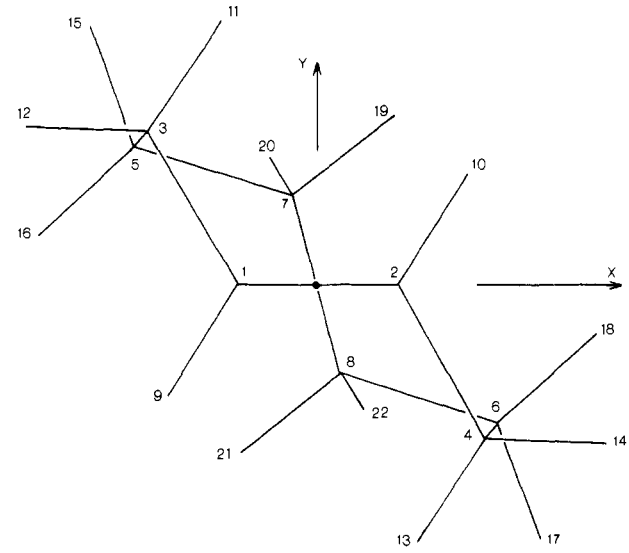

Figure 2. Structure and atom numbering for TCO.

improved virtual orbitals (IVO's) extracted from the computed amplitudes; the RPA formalism for this type of analysis is developed in section II and in the Appendix section. For the analysis of the mechanisms, we show in section III that the use of a localized orbital basis allows us to cast the RPA expression for the rotatory strength into a form containing all three contributions in Kirkwood's theory of optical rotatory power,[33,34] namely the one-electron model, the electric dipole–magnetic dipole (μ–m) coupling, and the polarizability theory (see ref 35 and 7 for surveys). This appears to be the first all-electron, ab initio formulation of optical rotatory power that allows a direct comparison among quantities modeling these early mechanisms.

In sections V and VI, we present results and detailed discussions for TCO and MCP and section VII contains an overall summary and concluding remarks.

II. Analyses of Computed Excitations

The RPA method we use to compute the excitation properties is described in detail elsewhere.[7,30] Briefly, the RPA is a method that includes those first-order correlation effects that are important for electronic intensities and excitation energies. In particular, the electric and magnetic dipole transition moments, which govern the ordinary and rotatory intensities (eq 17–21), are given by

$$\langle 0|\mathbf{r}|q\rangle = 2^{1/2}\sum_{\alpha}\sum_{m}\langle\phi_\alpha|\mathbf{r}|\phi_m\rangle\,(X_{\alpha m,q} + Y_{\alpha m,q}) \quad (1)$$

$$\langle 0|\tilde{\nabla}|q\rangle = 2^{1/2}\sum_{\alpha}\sum_{m}\langle\phi_\alpha|\tilde{\nabla}|\phi_m\rangle\,(X_{\alpha m,q} - Y_{\alpha m,q}) \quad (2)$$

$$\langle 0|\mathbf{r}\times\tilde{\nabla}|q\rangle = 2^{1/2}\sum_{\alpha}\sum_{m}\langle\phi_\alpha|\mathbf{r}\times\tilde{\nabla}|\phi_m\rangle\,(X_{\alpha m,q} - Y_{\alpha m,q}) \quad (3)$$

in the RPA.[30] Here ϕ_α and ϕ_m are, respectively, (real) occupied and virtual Hartree–Fock orbitals. The coefficients $X_{\alpha m,q}$ and $Y_{\alpha m,q}$ and the excitation energies ω_q are determined by a non-Hermitian eigenvalue problem,[30] and in a complete Hartree–Fock basis, the length and velocity forms of the electric dipole transition moment (eq 1 and 2) fulfill the hypervirial relation[7,36]

$$\langle 0|\tilde{\nabla}|q\rangle = \omega_q\langle 0|\mathbf{r}|q\rangle \quad (4)$$

The phase combinations $X_{\alpha m,q} \pm Y_{\alpha m,q}$ of the coefficients in eq 1–3 follow from the respective Hermitian and anti-Hermitian character of the transition moment operators, and the eigenvectors are orthonormal in the sense[37]

$$\sum_{\alpha}\sum_{m}\{X_{\alpha m,q}\,X^*_{\alpha m,p} - Y_{\alpha m,q}Y^*_{\alpha m,p}\} = \delta_{qp} \quad (5)$$

(23) Bouman, T. D.; Hansen, Aa. E. *J. Chem. Phys.* **1977**, *66*, 3460.
(24) Liskow, D. H.; Segal, G. A. *J. Am. Chem. Soc.* **1978**, *100*, 2945.
(25) Robin, M. B.; Basch, H.; Kuebler, N. A.; Kaplan, B. E.; Meinwald, J. *J. Chem. Phys.* **1968**, *48*, 5037.
(26) Yaris, M; Moscowitz, A.; Berry, R. S. *J. Chem. Phys.* **1968**, *49*, 3150.
(27) Rauk, A.; Jarvie, J. O.; Ichimura, K.; Barriel, J. M. *J. Am. Chem. Soc.* **1975**, *97*, 5656.
(28) Rauk, A.; Barriel, J. M. *Chem. Phys.* **1977**, *25*, 409.
(29) Hansen, Aa. E.; Bouman, T. D. *Mol. Phys.* **1979**, *37*, 1713.
(30) Bouman, T. D.; Hansen, Aa. E.; Voigt, B.; Rettrup, S. *Int. J. Quantum Chem.* **1983**, *23*, 595; *QCPE Bull.* **1983**, *3*, 63 (Program 459).
(31) McCurdy, C. W.; Rescigno, T. N.; Yeager, D. L.; McKoy, V. In "Methods of Electronic Structure Theory"; Schaefer, H. F., Ed.; *Plenum* Press: New York, 1977.
(32) Oddershede, J. *Adv. Quantum Chem.* **1978**, *11*, 275.
(33) Kirkwood, J. G. *J. Chem. Phys.* **1937**, *5*, 479.
(34) Kirkwood, J. G. *J. Chem. Phys.* **1939**, *7*, 139.
(35) Schellman, J. A. *Acc. Chem. Res.* **1968**, *1*, 144.
(36) Harris, R. A. *J. Chem. Phys.* **1969**, *50*, 3947.

An orbital promotion $\phi_\alpha \rightarrow \phi_m$ therefore contributes the amount

$$w_{\alpha m,q} = X^2_{\alpha m,q} - Y^2_{\alpha m,q} \quad (6)$$

to the excitation normalization. This quantity can be negative; however, negative $w_{\alpha m,q}$'s are necessarily small in stable RPA calculations.[37]

The quantity

$$W_{\alpha,q} = \sum_m w_{\alpha m,q} \quad (7)$$

is then the normalization contribution from all promotions out of orbital ϕ_α in a given excitation $0 \rightarrow q$, and

$$W_{m,q} = \sum_\alpha w_{\alpha m,q} \quad (8)$$

similarly measures the normalization contribution from all promotions into virtual orbital ϕ_m for this excitation. The weight factors in eq 6–8 combined with atomic orbital expansions of the molecular orbitals (see Appendix section) provide some insight into the nature of the excitations. However, for large, low-symmetry molecules and extended basis sets, such decompositions into atomic orbital contributions are not easily interpreted. Therefore, we summarize below a number of excitation characteristics that lend themselves to representation in the form of contour plots. Population analyses of these quantities are presented in the Appendix section.

Transition Densities. The transition moment induced by a general spin-free one-electron operator $\hat{F} = \sum_i \hat{f}_i$ can be expressed in terms of a transition density matrix[38] by the relation

$$\langle 0|\hat{F}|q\rangle = \int dV\, \hat{f}\, \rho_{0,q}(\mathbf{r}',\mathbf{r}) \quad (9)$$

Here $\hat{f}$ operates on $\mathbf{r}$ only, after which $\mathbf{r}'$ is set equal to $\mathbf{r}$ and the spatial integration is carried out. For $\hat{f}$ equal to the unit operator, eq 9 shows that the diagonal part of the transition density matrix integrates to zero:

$$\int dV\, \rho_{0,q}(\mathbf{r},\mathbf{r}) = 0 \quad (10)$$

For the purpose of analysis, the full six-dimensional transition density matrix $\rho_{0,q}(\mathbf{r}',\mathbf{r})$ is too unwieldy; we consider instead a representation in terms of its diagonal part, namely the three-dimensional transition density[38,39] $\rho_{0,q}(\mathbf{r}) \equiv \rho_{0,q}(\mathbf{r},\mathbf{r})$.

In the RPA, the transition density corresponding to eq 1 is[40]

$$\rho_{0,q}(\mathbf{r}) = 2^{1/2} \sum_\alpha \sum_m \phi_\alpha^*(\mathbf{r})\, \phi_m(\mathbf{r})\, (X_{\alpha m,q} + Y_{\alpha m,q}) \quad (11)$$

Since the operator in eq 1 is purely multiplicative, eq 11 determines the length form of the electric dipole transition moment completely. On the other hand, eq 2 and 3 contain differential operators; they are therefore determined by the off-diagonal parts of the matrix, and the corresponding transition density is not really relevant.

Most applications and interpretations of the transition density follow from the fact that its various electric multipole moments provide the corresponding transition moments. For molecules with nontrivial symmetry, $\rho_{0,q}(\mathbf{r})$ transforms as (a component of) the direct product of the irreducible representations of the states 0 and q. A particularly illustrative application of the use of this symmetry property is the work of Fischer-Hjalmars[41] on the vibronic intensities of electric dipole forbidden excitations. The distribution of transition density shows how different parts of the molecule contribute to the transition moment and hence serves to identify the effective electric dipole chromophore for a given excitation.

Rearrangement Densities. A different kind of density representation of an electronic excitation can be obtained from the following RPA expression for the expectation value difference for a general one-electron operator:[42]

$$\langle q|\hat{F}|q\rangle - \langle 0|\hat{F}|0\rangle = \sum_{\alpha m}\sum_{\beta n} \{\langle m|\hat{f}|n\rangle \delta_{\alpha\beta} - \langle \alpha|\hat{f}|\beta\rangle \delta_{mn}\} \Xi^q_{\alpha m,\beta n} \quad (12a)$$

with

$$\Xi^q_{\alpha m,\beta n} = X^*_{\alpha m,q} X_{\beta n,q} + Y^*_{\alpha m,q} Y_{\beta n,q} \quad (12b)$$

For $\hat{f}$ equal to the one-electron density operator $\delta(\mathbf{r} - \mathbf{r}')$, eq 12a provides the rearrangement density[43]

$$\Delta_{0,q}(\mathbf{r}) = \sum_{\alpha m}\sum_{\beta n} \{\phi^*_m(\mathbf{r})\phi_n(\mathbf{r})\delta_{\alpha\beta} - \phi^*_\alpha(\mathbf{r})\phi_\beta(\mathbf{r})\delta_{mn}\} \Xi^q_{\alpha m,\beta n} \quad (13)$$

It follows that

$$\int dV\, \Delta_{0,q}(\mathbf{r}) = 0 \quad (14)$$

The rearrangement density (eq 13) is the difference between the static electronic densities of states q and 0, and its electric dipole moment is the corresponding dipole moment difference. In fact, since the RPA computes excitation rather than state properties, eq 12 and 13 provide the only route to upper-state static properties within this method.[42]

Improved Virtual Orbitals. A number of different orbital promotions normally contribute significantly to the normalization and transition density of given excitation. However, for some excitations, the contribution $W_{\alpha,q}$ (eq 7) from a particular orbital (the bonding π orbital for most of the low-lying excitations in the monoolefins studied here) accounts for almost the entire normalization. The transition density (eq 11) can then be approximated by

$$\rho_{0,q}(\mathbf{r}) \simeq 2^{1/2} \phi^*_\alpha(\mathbf{r}) \mathrm{IVO}_\alpha^q(\mathbf{r}) \quad (15)$$

where $\phi_\alpha(\mathbf{r})$ is the bonding orbital that dominates the normalization of this excitation and where the excitation-specific function

$$\mathrm{IVO}_\alpha^q(\mathbf{r}) = \sum_m \phi_m(\mathbf{r})(X_{\alpha m,q} + Y_{\alpha m,q}) \quad (16)$$

is the RPA version[40] of an improved virtual orbital (IVO).[29,70]

(37) Rowe, D. J. *Rev. Mod. Phys.* **1968**, *40*, 153.
(38) McWeeny, R.; Sutcliffe, B. "Methods of Molecular Quantum Mechanics", 2nd ed.; Academic Press: New York, 1976.
(39) Sommerfeld, A. "Atombau und Spectrallinien. Wellenmechanischer Ergänzungsband", Fr. Vieweg u. Sohn: Braunschweig, 1929.
(40) Larson, E. G. *Int. J. Quantum Chem.* **1978**, *13*, 743.
(41) Fischer-Hjalmars, I. *J. Mol. Spec.* **1971**, *39*, 321.
(42) Lynch, D.; Herman, M. F.; Yeager, D. L. *Chem. Phys.* **1982**, *64*, 69.
(43) We prefer the term rearrangement density to difference density, because the latter is commonly used for the difference between molecular density and superposed atomic densities.
(44) Stiles, P. J. *Mol. Phys.* **1971**, *22*, 731.
(45) Bouman, T. D.; Voigt, B.; Hansen, Aa. E. *J. Am.* Chem. *Soc.* **1979**, *101*, 550.
(46) For simplicity, the term bond includes lone-pair orbitals.
(47) Howell, J. M. *J. Chem. Phys.* **1970**, *53*, 4152.
(48) Lightner, D. A.; Bouman, T. D.; Wijekoon, W. M. D.: Hansen, Aa. E. *J. Am. Chem. Soc.* **1984**, *106*, 934.
(49) Bendazzoli, G.; Biscarini, P.; Palmieri, P.; Gottarelli, G. *J. Chem. Soc., Faraday Trans. 2* **1981**, *77*, 503.
(50) Akagi, K.; Yamabe, T.; Kato, H.; Imamura, A.; Fukui, K. *J. Am. Chem. Soc.* **1980**, *102*, 5157.
(51) Condon, E. J.; Altar, W.; Eyring, K. *J. Chem. Phys.* **1937**, *5*, 753.
(52) Moscowitz, A. *Adv. Chem. Phys.* **1962**, *4*, 67.
(53) Moffitt, W. *J. Chem. Phys.* **1956**, *25*, 467.
(54) Moscowitz, A.; Hansen, Aa. E.; Forster, L. S.; Rosenheck, K. *Biopolymers* **1964**, *S1*, 75.
(55) Woody, R. W.; Tinoco, I. *J. Chem. Phys.* **1967**, *46*, 4927.
(56) Bayley, P.; Nielsen, E. B.; Schellman, J. A. *J. Phys. Chem.* **1969**, *73*, 228.
(57) Schippers, P. H.; Dekkers, H. P. J. M. *J. Am. Chem. Soc.* **1983**, *105*, 79.
(58) (a) Buckingham, A. D.; Stiles, P. J. *Acc. Chem. Res.* **1974**, *7*, 258. (b) Applelquist, J. *Acc. Chem. Res.* **1977**, *10*, 79. (c) Sundberg, K. R. *J. Chem. Phys.* **1978**, *68*, 5271. (d) Barron, L. D. "Molecular Light Scattering and Optical Activity"; Cambridge University Press: New York, 1982.
(59) Allinger, N. L. *J. Am. Chem. Soc.* **1977**, *99*, 8127.
(60) (a) Traetteberg, M. *Acta Chem. Scand., Ser. B* **1975**, *B29*, 29. (b) Traetteberg, M.; Bakken, P.; Almenningen, A. *J. Mol. Struct.* **1981**, *74*, 321.
(61) Van Kampen, P. N.; de Leeuw, F. A. A. M.; Smits, G. F.; Altona, C. Program QCPE 437, Quantum Chemistry Program Exchange, Indiana University, 1982. Pople, J. A., et al. *QCPE* **1981**, *406*.

In such cases, the IVO_α^q provides an immediate illustration (assignment) of the nature of the upper state. An improved ground orbital[27] IGO_m^q can be defined analogously to describe excitations predominantly into one particular virtual orbital; however, such excitations appear to be uncommon in extended basis set calculations.

Comments. Equation 13 represents what is commonly envisaged as the motion of charge accompanying an electronic excitation. However, it is important to emphasize that the transition density $\rho_{0,q}(\mathbf{r})$ and the rearrangement density $\Delta_{0,q}(\mathbf{r})$ are mathematically independent quantities and provide very different types of information. Specifically, $\rho_{0,q}(\mathbf{r})$ is manifestly nonclassical, since it is determined only up to a phase factor, and as mentioned above, it can transform as any of the irreducible representations of the molecular point group. On the other hand, $\Delta_{0,q}(\mathbf{r})$ can be treated as a classical electronic charge distribution and is totally symmetric regardless of the transformation properties of the states 0 and q. The distinction is exemplified by the $n \rightarrow \pi^*$ excitation in ketones where the electric dipole moment of the transition density is almost zero, whereas the dipole moment of the rearrangement density may be several debyes.

From a structural point of view, features (or changes) in regions of large values of $\rho_{0,q}(\mathbf{r})$ will be of particular importance for the intensities of excitation $0 \rightarrow q$, whereas features (or changes) in regions of large $\Delta_{0,q}(\mathbf{r})$ will affect the excitation energy. These respective regions can also be identified from the gross atomic populations defined in the Appendix section. However, the quantitative value of these populations is somewhat limited because the Mulliken approximation (eq A4) quenches important one-center terms, in particular the atomic 2s, 2p dipole moment contribution. In addition, the atomic orbital expansions of the densities are not easily interpreted for extended basis sets. We shall accordingly make use of contour diagrams to represent densities and orbitals.

III. Analysis of Computed Intensities

The oscillator strength is obtained from the transition moments in eq 1–3 by one of the following equivalent expressions[7] (in atomic units)

$$f_{0,q}{}^{\nabla} = \tfrac{2}{3}\omega_q{}^{-1}|\langle 0|\hat{\nabla}|q\rangle|^2 \tag{17}$$

$$f_{0,q}{}^{r\nabla} = \tfrac{2}{3}\langle 0|\hat{\nabla}|q\rangle\cdot\langle 0|\mathbf{r}|q\rangle \tag{18}$$

$$f_{0,q}{}^{r} = \tfrac{2}{3}\omega_q|\langle 0|\mathbf{r}|q\rangle|^2 \tag{19}$$

and the rotatory strength is similarly determined by the expressions (in atomic units)

$$R_{0,q}{}^{\nabla} = (1/2c)\omega_q{}^{-1}\langle 0|\hat{\nabla}|q\rangle\cdot\langle 0|\mathbf{r}\times\hat{\nabla}|q\rangle \tag{20}$$

$$R_{0,q}{}^{r} = (1/2c)\langle 0|\mathbf{r}|q\rangle\cdot\langle 0|\mathbf{r}\times\hat{\nabla}|q\rangle \tag{21}$$

In complete RPA calculations, the validity of eq 4 ensures that eq 17–19 and eq 20 and 21, respectively, yield identical results.

General Decompositions. The transition density (eq 11) illustrates the contributions of different parts of the molecule to the electric dipole transition moment. However, the magnetic dipole transition moment and its contributions cannot easily be visualized this way, and more seriously, these quantities are not well-defined[7,44] as shown in eq 28 below. Furthermore, for structural purposes, the main interest lies in extracting intensity mechanisms, i.e., the way that different parts of a molecule interact to generate the total intensities. To this end, we now assume that the occupied molecular orbitals ϕ_α are localized, with centroids defined by

$$\rho_\alpha = \langle\phi_\alpha|\mathbf{r}|\phi_\alpha\rangle \tag{22}$$

The RPA equations, and thus the formalism developed so far, are equally applicable to both canonical and localized bases;[45] from eq 1–3, we can then introduce the excitation-characteristic bond[46] transition moments

$$\mathbf{r}_{\alpha,q} = 2^{1/2}\sum_m \langle\phi_\alpha|\mathbf{r}|\phi_m\rangle\ (X_{\alpha m,q} + Y_{\alpha m,q}) \tag{23}$$

$$\nabla_{\alpha,q} = 2^{1/2}\sum_m \langle\phi_\alpha|\hat{\nabla}|\phi_m\rangle\ (X_{\alpha m,q} - Y_{\alpha m,q}) \tag{24}$$

$$\ell_{\alpha,q} = 2^{1/2}\sum_m \langle\phi_\alpha|\mathbf{r}\times\hat{\nabla}|\phi_m\rangle\ (X_{\alpha m,q} - Y_{\alpha m,q}) \tag{25}$$

Equations 23–25 are invariant to unitary transformations within the virtual space, so that it is immaterial for these bond moments whether the virtual orbitals are localized or canonical.

The oscillator strengths in eq 17–19 then reduce to various products of the electric dipole length and velocity bond moments in eq 23 and 24. However,

$$\nabla_{\alpha,q} \neq \omega_q\mathbf{r}_{\alpha,q} \tag{26}$$

even in complete bases where eq 4 is fulfilled, so that eq 17 and 19 will tend to overemphasize, respectively, the length and velocity contributions in decomposition. A suitable compromise is

$$f_{0,q}{}^{r\nabla} = \tfrac{1}{3}\sum_{\alpha,\beta}\{\nabla_{\alpha,q}\cdot\mathbf{r}_{\beta,q} + \nabla_{\beta,q}\cdot\mathbf{r}_{\alpha,q}\} \equiv \sum_{\alpha,\beta} f_{\alpha\beta}{}^q \tag{27}$$

from eq 18 which also ensures that the individual bond–bond contributions $f_{\alpha\beta}{}^q$ are symmetrized in the bond indexes.

For the rotatory strengths, eq 20 and 21 produce the products $\nabla_{\alpha,q}\cdot\ell_{\beta,q}$ and $\mathbf{r}_{\alpha,q}\cdot\ell_{\beta,q}$ from eq 23–25. These terms are not well-defined individually because a translation of the coordinate origin corresponding to $\mathbf{r} \rightarrow \mathrm{r} - \mathbf{a}$ changes the magnetic dipole transition moment according to

$$\ell_{\beta,q} \rightarrow \ell_{\beta,q} - \mathbf{a}\times\nabla_{\beta,q} \tag{28}$$

while $\mathbf{r}_{\alpha,q}$ and $\nabla_{\alpha,q}$ are left unchanged. Since $\nabla_{\alpha,q}$ and $\mathbf{r}_{\alpha,q}$ are not parallel to $\nabla_{\beta,q}$ in general, the product $\nabla_{\alpha,q}\cdot\ell_{\beta,q}$ can therefore be given (almost) any value by arbitrarily changing the origin. For eq 20, this problem is handled by writing

$$R_{0,q} = (1/4c)\omega_q{}^{-1}\sum_{\alpha,\beta}\{\nabla_{\alpha,q}\cdot\ell_{\beta,q} + \nabla_{\beta,q}\cdot\ell_{\alpha,q}\} \equiv \sum_{\alpha,\beta} R_{\alpha\beta}{}^q. \tag{29}$$

The origin terms generated by eq 28 cancel for the symmetric combination of the products, making $R_{\alpha\beta}{}^q$ (and of course $R_{0,q}{}^{\nabla}$)[7] origin-invariant, regardless of basis set quality. On the other hand, eq 26 shows that a corresponding symmetric combination of the products $\mathbf{r}_{\alpha,q}\cdot\ell_{\beta,q}$ is not origin-invariant; eq 21 is hence inappropriate for decompositions, even in complete bases where eq 4 makes $R_{0,q}{}^{r}$ itself invariant. Decomposition of rotatory strengths into symmetric contributions was first used by Howell,[47] and similar analyses have been presented recently by us[48] and by Bendazzoli et al.;[49] the configuration interaction analysis given by Akagi et al.[50] apparently overlooks the origin problem.

Kirkwood Approach. As stressed above, when all transition moments are referred to a central molecular coordinate system, eq 28 prevents identification of individual electric and magnetic dipole contributions to the bond–bond coupling terms $R_{\alpha\beta}{}^q$ (eq 29); only the symmetrized electric dipole–magnetic dipole contributions are computationally meaningful. On the other hand, supposedly meaningful local electric and magnetic contributions have been invoked in almost all models of molecular optical rotatory power ever since Kirkwood's 1937 paper.[33,34] To establish a connection to such approaches, we expand the magnetic bond

(62) (a) A summary of the implementation of the optical integrals is given in: Hansen, Aa. E.; Bouman, T. D. *J. Chem. Phys.* **1985**, *82*, 5035. (b) Our results on planar monoolefins are found in: Bouman, T. D.; Hansen, Aa. E. *Chem. Phys. Lett.*, in press.

(63) Dunning, T. H.; Hay, P. J. In "Methods in Electronic Structure Theory"; Schaefer, H. F., Ed.; Plenum Press: New York, 1977.

(64) Huzinaga, S. *J. Chem. Phys.* **1965**, *42*, 1293.

(65) Dunning, T. H.; McKoy, V. *J. Chem. Phys.* **1967**, *47*, 1735.

(66) The (−) enantiomer has served as the model for nearly all calculations in the literature; the published CD spectrum in ref 3 is on the (+) form.

(67) For an example of the effect of going beyond the RPA, see: Jørgensen, P.; Oddershede, J. *J. Chem. Phys.* **1983**, *78*, 1898.

(68) Binkley, J. S.; Pople, J. A. *Int. J. Quantum Chem.* **1975**, *9*, 229.

(69) Gedanken, A.; Kuebler, N. A.; Robin, M. B. *J. Chem. Phys.* **1982**, *76*, 46.

(70) We use the term IVO only in the sense of a linear combination of SCF virtual orbitals that allows a computed excitation to be expressed approximately as a single orbital promotion; in the present context, an IVO is an entirely *a posteriori* construct used as an aid in assigning the nature of the excitation.

transition moment (eq 25) relative to the corresponding bond centroid

$$\ell_{\alpha,q} = 2^{1/2}\sum_m \langle\phi_\alpha|(\mathbf{r}-\rho_\alpha)\times\nabla|\phi_m\rangle\,(X_{\alpha m,q} - Y_{\alpha m,q}) + \rho_\alpha \times \nabla_{\alpha,q} \equiv \ell'_{\alpha,q} + \rho_\alpha \times \nabla_{\alpha,q} \quad (30)$$

from eq 22 and 24. $\ell'_{\alpha,q}$ is now an inherent magnetic bond transition moment, and the second term in eq 30 is a "moment of momentum" term. Equation 30 allows us to write a bond–bond coupling term $R_{\alpha\beta}{}^q$ from eq 29 in the form

$$R_{\alpha\beta}{}^q = (1/4c)\omega_q{}^{-1}\,\nabla_{\alpha,q}\cdot\ell'_{\beta,q} + (1/4c)\omega_q{}^{-1}\,\nabla_{\beta,q}\cdot\ell'_{\alpha,q} + (1/4c)\omega_q{}^{-1}(\rho_\alpha - \rho_\beta)\cdot(\nabla_{\alpha,q}\times\nabla_{\beta,q}) \quad (31)$$

where all three terms are manifestly origin-independent.

Equation 31 has the same structure as the Kirkwood theory of optical activity.[33,34] Consider first a diagonal term

$$R_{\alpha\alpha}{}^q = (1/2c)\omega_q{}^{-1}\,\nabla_{\alpha,q}\cdot\ell'_{\alpha,q} \equiv R_\alpha{}^q(\text{intr.}) \quad (32)$$

This is an intrinsic bond contribution, and within the present formalism, such terms represent the one-electron mechanism[35,51] which in turn can be interpreted in terms of inherent dissymmetry or dissymmetric (static) perturbations[52] by inspection of the degree of dissymmetry (e.g., twist) of orbital ϕ_α. The computed value of eq 32 does not by itself distinguish between these two classifications.

For $\alpha \neq \beta$, all three contributions in eq 30 come into play. A contribution to the form

$$R^q(\mu_\alpha,m_\beta) = (1/4c)\omega_q{}^{-1}\,\nabla_{\alpha,q}\cdot\ell'_{\beta,q} \quad (33)$$

represents the coupling between an electric dipole transition moment (μ) for bond α and an intrinsic magnetic dipole moment (m) for bond β.[35] Notice that $R^q(\mu_\alpha,m_\beta)$ and $R^q(\mu_\beta,m_\alpha)$ are now two distinctly different, well-defined coupling contributions. Such terms were assumed negligible by Kirkwood,[33] and conditions for the validity of this assumption were discussed later by Moffitt[53] and Stiles[44] (see also ref 35 and 7). Explicit semiempirical studies of these coupling terms have indicated that they can actually dominate the rotatory strengths for some types of excitation.[54–57]

Finally, the μ–μ coupling

$$R^q(\mu_\alpha,\mu_\beta) = (1/4c)\omega_q{}^{-1}\,(\rho_\alpha - \rho_\beta)\cdot(\nabla_{\alpha,q}\times\nabla_{\beta,q}) \quad (34)$$

has the form of the polarizability contributions that are commonly identified with Kirkwood's theory and which still form the basis for a number of approaches to optical activity.[58] The absence of any reference to individual excited configurations in eq 34 removes the distinction between degenerate (exciton-like) couplings and nondegenerate (polarizability-type) couplings[7] in the present formulation.

In summary, eq 31–34 provide a decomposition of computed rotatory strengths into easily recognizable and structurally meaningful coupling terms, involving no approximations beyond those entering the RPA method used to compute the excitation properties. The relative simplicity of this formulation is obtained by relinquishing information about contributions from promotions into individual virtual orbitals, through the introduction of the effective bond transition moments (eq 23–26). The price paid for this simplification is some loss of distinctions, notably between degenerate and nondegenerate μ–μ couplings and between local and charge-transfer contributions. However, the latter distinction is not really computationally clear-cut, because the localized virtual orbitals required in this context are much less compact than their occupied counterparts, especially in extended basis sets. Hence, although the overall local or charge-transfer nature of an excitation can be gleaned from the quantities discussed in section II, we refrain here from analyses of the intensities into such contributions.

IV. Computational Details and Overall Results

Geometries. The TCO geometry (Figure 2 and Table I) was obtained from a molecular mechanics optimization based on Allinger's 1977 force field (MM2),[59] using Traetteberg's electron diffraction parameters[60] as input and with dihedral angles appropriate for (−)-TCO. The relaxations provided by the MM2 optimization were within the standard deviations given by Traetteberg.[60] The TCO-distorted geometries of ethylene and *trans*-2-butene were generated by replacing, respectively, C_1–C_3 and C_2–C_4 by C–H bonds of length 1.09 Å and C_3–C_5 and C_4–C_6 by C–H bonds of length 1.12 Å. The Cartesian coordinate system for all calculations reported here is centered on the C=C bond, with the x direction along the bond and z perpendicular to the (ethylene) molecular plane; the z axis is thus retained as a symmetry axis in TCO and its fragments. With this coordinate system, x transforms as B_{1u} for planar ethylene.

Table I. Unique Geometrical Parameters for TCO (C_2 symmetry). Atom Numbering Shown in Figure 2

bond lengths, Å	bond angles, deg	dihedral angles, deg
$r(C_1–C_2)$ = 1.332	$C_3–C_1–C_2$ = 118.9	$C_3–C_1–C_2–C_4$ = 214.7
$r(C_1–C_3)$ = 1.498	$C_5–C_3–C_1$ = 103.6	$H–C_1–C_2–H$ = 188.9
$r(C_3–C_5)$ = 1.547	$C_7–C_5–C_3$ = 116.2	$C_5–C_3–C_1–C_2$ = 87.6
$r(C_5–C_7)$ = 1.554	$H–C_1–C_2$ = 120.7	$C_7–C_5–C_3–C_1$ = −47.6
$r(C_1–H)$ = 1.104	$H_{11}–C_3–C_1$ = 111.6	$H_{11}–C_3–C_1–C_2$ = −30.9
$r(C_3–H)$ = 1.116	$H_{12}–C_3–C_1$ = 111.1	$H_{12}–C_3–C_1–C_2$ = −151.7
$r(C_5–H)$ = 1.117	$H_{15}–C_5–C_3$ = 107.2	$H_{15}–C_5–C_3–C_1$ = −170.3
$r(C_7–H_{19})$ = 1.114	$H_{16}–C_5–C_3$ = 109.5	$H_{16}–C_5–C_3–C_1$ = 75.3
$r(C_7–H_{20})$ = 1.117	$H_{19}–C_7–C_5$ = 110.3	$H_{19}–C_7–C_5–C_3$ = −50.8
	$H_{21}–C_7–C_5$ = 105.4	$H_{20}–C_7–C_5–C_3$ = −162.5

Table II. Cartesian Coordinates (in Å) for Equatorial (MCPE) and Axial (MCPA) (3*R*)-3-Methylcyclopentene, as Used in This Work. Atom Numbering Shown in Figure 1

	equatorial			axial		
atom	x	y	z	x	y	z
C_1	−0.667	0.0	0.0	−0.669	0.0	0.0
C_2	0.667	0.0	0.0	0.669	0.0	0.0
C_3	1.228	1.398	0.0	1.237	1.396	−0.008
C_4	0.003	2.236	0.406	0.0	2.226	−0.408
C_5	−1.221	1.398	0.0	−1.233	1.394	0.0
C_6	2.433	1.560	0.926	1.749	1.770	1.403
H_7	−1.282	−0.902	−0.062	−1.299	−0.904	0.026
H_8	1.284	−0.900	−0.064	1.299	−0.904	0.022
H_9	1.497	1.610	−1.048	2.055	1.493	−0.747
H_{10}	0.005	3.248	−0.024	0.002	2.325	−1.521
H_{11}	0.008	2.345	1.500	−0.007	3.257	0.017
H_{12}	−2.052	1.492	0.712	−1.588	1.648	1.026
H_{13}	−1.545	1.618	−1.209	−2.070	1.504	−0.728
H_{14}	3.281	0.958	0.575	2.582	1.098	1.715
H_{15}	2.191	1.227	1.942	0.943	1.694	2.168
H_{16}	2.741	2.613	0.963	2.135	2.815	1.416

For MCP, we used the Cartesian coordinates listed by Levi et al.[20] as initial geometry in an MM2 optimization. The resulting relaxations were quite extensive, yielding a pronounced equatorial methyl position (MCPE: Figure 1 and Table II), in contrast to the geometry of Levi et al. where the C_3–C_6 and C_3–H_9 bonds are nearly symmetrically disposed with respect to the C_5–C_1–C_2–C_3 plane. Where there is an equatorial conformation, there is also an axial conformation (MCPA), and an MM2 optimization of the latter yields a steric energy only 0.2 kcal/mol larger than the energy of the equatorial form. We have accordingly included both conformations in this study, and the MCPA coordinates are also listed in Table II.

Computations and Basis Sets. All calculations reported here were done with a version of GAUSSIAN 80[61] modified to provide the necessary optical integrals[62] and of RPAC[30] extended to encompass the analyses described in sections II and III. The atomic basis set used for carbon is the [3s2p] Gaussian set of Dunning and Hay,[63] supplemented by split diffuse 3s (α_s = 0.044 and α'_s = 0.017) and 3p (α_p = 0.040 and α'_p = 0.016) Gaussians. For the hydrogens, we used the Dunning and Hay [2s] contraction.[63] All hydrogen orbitals are scaled by 1.20, while the carbon functions are unscaled. This basis set, termed basis A, was used for calculations on the TCO-distorted ethylene and *trans*-2-butene (see also ref 62b). Computational limitations precluded the use of this basis in TCO and MCP. Accordingly, a modified basis called basis B was constructed from basis A by retaining the diffuse

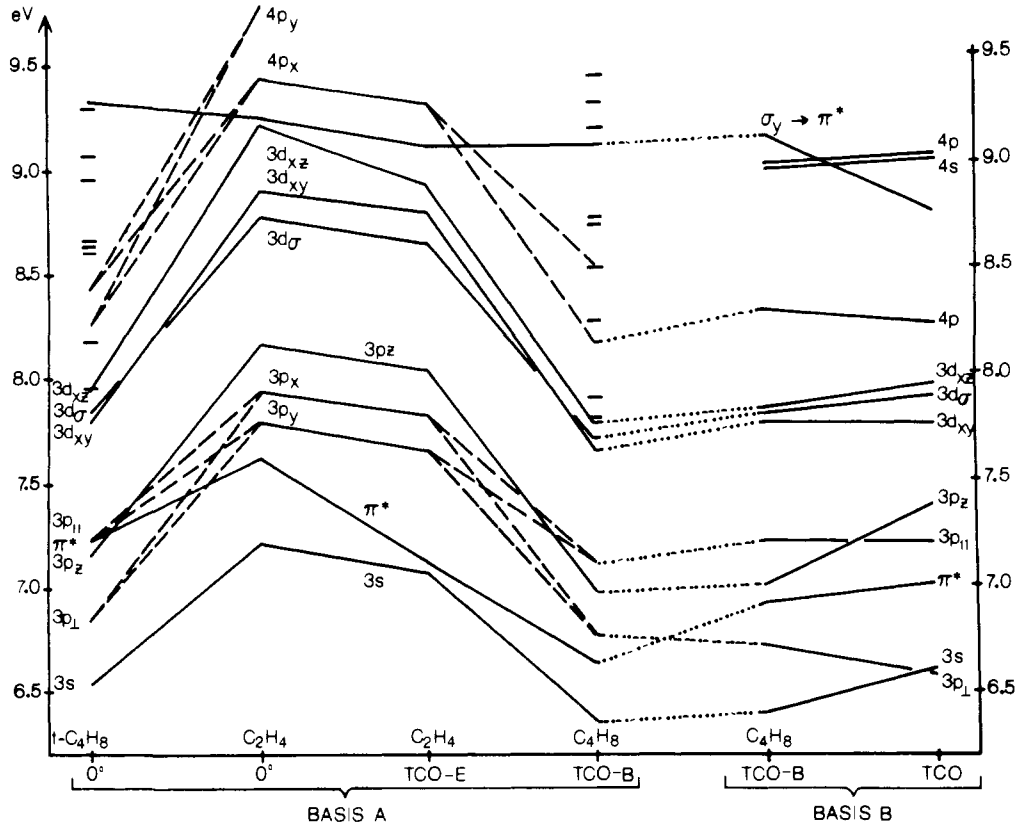

Figure 3. Correlation diagram for low-lying singlet excitations in TCO and its fragments. Except as indicated, all assignments refer to excitations out of bonding π orbital. The designations "0°" and "TCO" refer to the planar and TCO-like conformations, respectively, of the indicated molecules.

Table III. SCF Energies for the Molecules Studied (in hartrees)

molecule	basis	energy
ethylene	A, B	-78.012995
TCO-E	A, B	-77.997513
TCO-B	A	-156.041156
TCO-B	B	-156.035453
TCO	B	-310.934428
MCPA	B	-232.928305
MCPE	B	-232.931752

functions only on the two chromophore carbons and by replacing the [2s] basis with a single (5s)/[1s] contracted function[64] on all hydrogens except those directly bonded to C=C.

With these bases, ethylene and butene are spanned by, respectively, 42 and 84 atomic basis functions in basis A, while butene, TCO, and MCP are spanned by, respectively, 62, 104, and 82 contracted basis functions in basis B. Table III contains the SCF energies obtained with these bases. Occupied orbitals were localized according to the Foster–Boys criterion followed by redelocalization of "banana" orbitals into their σ and π counterparts.[45] The occupied orbital centroid positions correspond closely to the midpoints of the respective bonds. Virtual orbitals were used directly as they came from the SCF step. When excitations out of the carbon 1s orbitals are excluded, the resulting RPA calculations for TCO (MCP) include 1679 (1003) singly excited configurations. The effects of as many as 700 000 doubly excited configurations on the excitations are implicitly accounted for in the RPA, primarily through the Y coefficients.

Overall Results. Figures 3 and 4 display an overview of our monoolefin results in the form of correlation diagrams, and Table IV presents results for planar ethylene to establish a base line. We note that the $\pi \rightarrow \pi^*$ excitation energy is particularly sensitive to the diffuse part of the atomic basis set. The use of a split diffuse basis is essential for the $\pi \rightarrow \pi^*$ agreement in Table IV, and Figures 3 and 4 show that this transition is more susceptible to basis set reduction in butene than are the Rydberg excitations. Further details on the planar monoolefins in these diagrams and comparison with other calculations are given in ref 62b. The

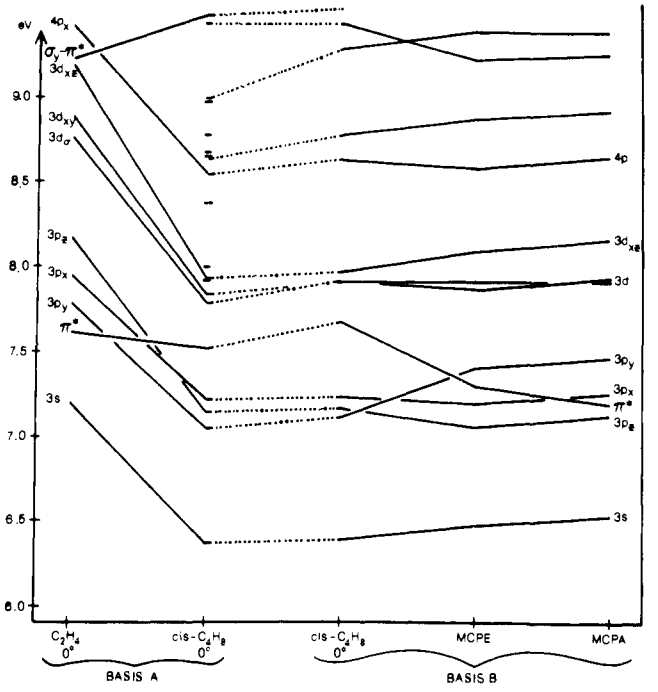

Figure 4. Correlation diagram for low-lying singlet excitations in MCP and related molecules. Assignments indicated as in Figure 3.

agreement in Table IV between computed and experimental energies and assignments is seen to be very satisfactory.

The results for the individual molecules are discussed in the following sections. As general trends, we note that all excitations apart from the high-lying excitation labeled $\sigma_y \rightarrow \pi^*$ are predominantly IVO-type, originating from the bonding π orbital. The assignments therefore refer to the character of the appropriate IVO's. The bonding orbital labeled σ_y has b_{3g} symmetry in planar ethylene and is bonding between C and H but antibonding across

Table IV. Low-Lying Singlet Electronic Excitations for Planar Ethylene: Computed RPA Results and Comparisons with Other Work

	exptl		this work		LS[b]			
excitation	ΔE[a]	f	ΔE	$f^{r\nabla}$	ΔE	$f^{r\nabla}$	PBP[c] ΔE	Na[d] ΔE
$B_{3u}(\pi \rightarrow 3s)$	7.14[e,f]	0.04	7.21	0.10	7.30	0.11	7.13	7.33
$B_{1u}(V, \pi \rightarrow \pi^*)$	7.66[e]	0.34	7.61	0.38	8.33	0.30	8.06	8.17
$B_{1g}(\pi \rightarrow 3p_y)$	7.80[e,f]		7.79		7.92		7.89	7.86
$B_{2g}(\pi \rightarrow 3p_x)$	8.00[e,f]		7.94				7.86	7.93
$A_g(\pi \rightarrow 3p_z)$	8.26[e,f]		8.16				8.21	8.28
$B_{3u}(\pi \rightarrow 3d_\sigma)$	8.62[e]		8.77	0.02	8.80	0.04	8.73	8.90
$A_u(\pi \rightarrow 3d_{xy})$			8.90				8.83	9.05
$B_{1u}(\pi \rightarrow 3d_{xz})$			9.21	0.03			9.17	9.60
$B_{1g}(\sigma_y \rightarrow \pi^*)$	9.9[e], 9.2?[e]		9.24		8.90			

[a] Energies in eV. [b] Reference 24. [c] Reference 17. [d] Reference 18. [e] Reference 4. [f] Reference 69.

Table V. Computed Excitation Energies and Intensities for (−)-TCO and Its Fragments

C_2H_4[a] (TCO-E)				C_4H_8[a] (TCO-B)				C_8H_{14}						
											$R^\nabla(10^{-40}$ cgs)			
b	ΔE, eV	$f^{r\nabla}$	$R^\nabla(10^{-40}$ cgs)	b	ΔE, eV	$f^{r\nabla}$	$R^\nabla(10^{-40}$ cgs)	b	ΔE, eV	$f^{r\nabla}$	tot	intrins[c]	μ-m[d]	μ-μ[e]
$\pi \rightarrow 3s$	7.07	0.08	−35	$\pi \rightarrow 3s$	6.40	0.01	−5	$\pi \rightarrow 3p_\perp$	6.58	0.05	−6	4	−2	−6
$\pi \rightarrow \pi^*$	7.12	0.29	−114	$\pi \rightarrow 3p_\perp$	6.72	0.03	6	$\pi \rightarrow 3s$	6.61	0.03	−5	−2	−1	−2
$\pi \rightarrow 3p_y$	7.65	0.00	−2	$\pi \rightarrow \{3p_\parallel, \pi^*\}$	6.92	0.15	−1	$\pi \rightarrow \pi^*$	7.06	0.22	−52	−13	−17	−22
$\pi \rightarrow 3p_x$	7.82	0.01	1	$\pi \rightarrow 3p_z$	7.00	0.02	2	$\pi \rightarrow 3p_\parallel$	7.21	0.02	32	14	−9	27
$\pi \rightarrow 3p_z$	8.03	0.01	0	$\pi \rightarrow \{\pi^*, 3p_\parallel\}$	7.22	0.11	−80	$\pi \rightarrow 3p_z$	7.38	0.00	0	0	0	0
$\pi \rightarrow 3d_\sigma$	8.64	0.02	−11	$\pi \rightarrow 3d_{xy}$	7.78	0.00	−1	$\pi \rightarrow 3d_{xy}$	7.77	0.00	−1	0	−1	0
$\pi \rightarrow 3d_{xy}$	8.79	0.00	0	$\pi \rightarrow 3d_\sigma$	7.81	0.01	0	$\pi \rightarrow 3d_\sigma$	7.89	0.01	12	4	0	8
$\pi \rightarrow 3d_{xz}$	8.92	0.03	80	$\pi \rightarrow 3d_{xz}$	7.84	0.04	4	$\pi \rightarrow 3d_{xz}$	7.95	0.01	−12	−5	−2	−5
$\sigma_y \rightarrow \pi^*$	9.10	0.05	71	$\pi \rightarrow 4p'$	8.31	0.01	−15	$\pi \rightarrow 4p'$	8.24	0.00	−9	0	−5	−4
$\pi \rightarrow 4p'_x$	9.30	0.00	3	$\pi \rightarrow 4s'$	8.98	0.01	−13	$\sigma_y \rightarrow \pi^*$	8.77	0.04	47	7	19	21
				$\pi \rightarrow 4p'$	8.99	0.00	−2	$\pi \rightarrow 4s'$	9.02	0.02	−26	−7	1	−18
				$\sigma_y \rightarrow \pi^*$	9.23	0.09	64	$\pi \rightarrow 4p'$	9.02	0.00	−2	−2	2	−1

[a] Distorted as in TCO. [b] IVO assignments; see Figure 3 for correlation diagram. [c] Total contributions from eq 32. [d] Total contributions from eq 33. [e] Total contributions from eq 34.

the XZ and YZ planes. Among the correlations shown, the excitations labeled 3s, $3p_z$, and $\sigma_y \rightarrow \pi^*$ retain their character in an easily recognizable form in all the systems, whereas the $\pi \rightarrow \pi^*$ excitation and the remaining Rydberg excitations change quite markedly. This is particularly pronounced for the two 3p excitations which transform as x and y in planar ethylene for symmetry reasons, whereas they become quantized perpendicular ($3p_\perp$) and parallel ($3p_\parallel$) to the effective molecular long axis ($\perp C_2$) in TCO and *trans*-butene. The $\sigma_y \rightarrow \pi^*$ transition, which we find to be quite valencelike, is much less sensitive to distortion and alkyl substitution than the other olefin excitations. In MCP, the $\sigma_y \rightarrow \pi^*$ excitation does not occur among the lowest 15 excitations, because of the increased density of states in the 8-eV region.

V. *trans*-Cyclooctene

We shall discuss the results for TCO together with those for its butene (TCO-B) and ethylene (TCO-E) fragments, in order to provide a context for comparisons with model calculations and to assess the extent to which the saturated parts of TCO affect the observed spectrum. Both canonical and localized MO's are used in the analysis: the canonical MO's yield the most straightforward assignments of the nature of the excitations, following the formalism of section II, whereas the intensity mechanisms are analyzed in a localized occupied orbital picture as developed in section III.

The RPA results for the energies, oscillator, and rotatory strengths obtained in basis B are given in Table V; the assignments are discussed below, and we return to a comparison with experimental spectra later. In terms of other computations, a direct comparison of our results to those of Liskow and Segal[24] is possible only for the TCO-E fragment, since the full TCO results represent energy-shifted ethylene values. We agree within 0.1–0.2 eV for the $\pi \rightarrow$ Rydberg excitations, but our $\pi \rightarrow \pi^*$ and $\sigma_y \rightarrow \pi^*$ transitions are about 0.5 eV lower. The only ab initio calculation on TCO besides the present is the minimal basis calculation of Rauk, Barriel, and Ziegler[22] on only the $\pi \rightarrow \pi^*$ excitation, using a variety of methods. Their "first-order CI" method which is comparable to the RPA, yields $R = -104$ and $f = 0.27$.

For the assignments of these transitions, an effective IVO (eq 16) can be constructed in each case to represent the receiving

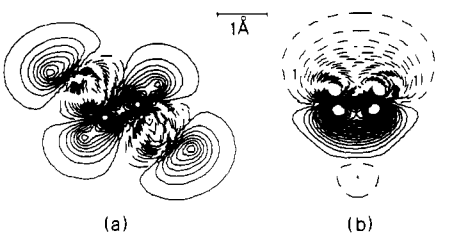

Figure 5. Contour plots of occupied orbitals in TCO involved in excitations: (a) σ_y, XY plane; (b) π, XZ plane. Dashed lines indicate regions of negative phase. Adjacent contours differ by a constant.

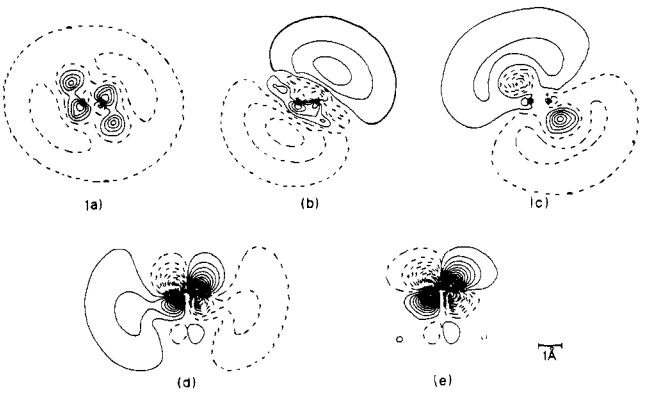

Figure 6. Contour plots of IVO's for TCO excitations: (a) 3s (XY plane); (b) $3p_\perp$ (XY plane); (c) $3p_\parallel$ (XY plane); (d) $(\pi \rightarrow)\pi^*$ (XZ plane); (e) $(\sigma_y \rightarrow)\pi^*$ (XZ plane).

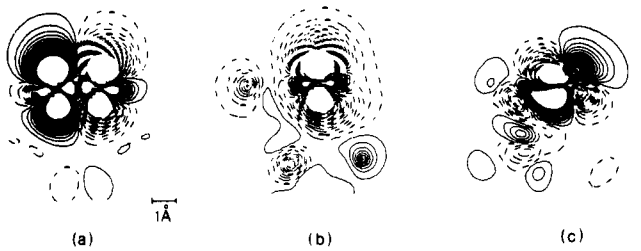

Figure 7. Contour plots of transition densities of TCO: (a) $\pi \rightarrow \pi^*$ (*XZ* plane); (b) $\pi \rightarrow \pi^*$ (*YZ* plane through C_2); (c) $\sigma_y \rightarrow \pi^*$ (*YZ* plane through midpoint of C_2–H_{10}).

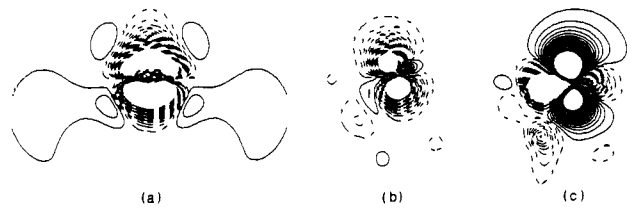

Figure 8. Contour plots of charge rearrangement densities of TCO. Planes defined as in Figure 7. Dashed lines indicate regions of net electron loss; solid lines show net gain.

orbital. Figure 5 shows contour plots of the occupied σ_y and π orbitals in TCO; the latter plot shows how the orthogonality of the π orbital to the rest of the occupied MO's forces it away from the back of the ring. Figure 6 displays contour plots of the effective IVO's for the $\pi \rightarrow 3s$, $\pi \rightarrow 3p_\perp$, $\pi \rightarrow 3p_\parallel$, $\pi \rightarrow \pi^*$, and $\sigma_y \rightarrow \pi^*$ excitations in TCO. These plots show that the two "in-plane" $\pi \rightarrow 3p$ transitions involve 3p-like orbitals which have been rotated in the *XY* plane relative to the C=C bond. This feature is present in both planar[62b] and TCO-distorted *trans*-2-butene; the Rydberg requantization is thus caused mainly by the nearest neighbors to the chromophore but is reinforced by the rest of the ring. As expected, the 3p IVO's in TCO-E are similar to those of planar ethylene[62b] and are quantized along the Cartesian axes. For $\pi \rightarrow \pi^*$ and $\sigma_y \rightarrow \pi^*$, the plots show that the effective receiving π^* orbitals in these two transitions are quite different.

Transition densities (eq 11) for $\pi \rightarrow \pi^*$ and $\sigma_y \rightarrow \pi^*$ excitations are shown in Figure 7. The $\pi \rightarrow \pi^*$ plot displays the expected large dipole moment along the C=C bond axis; notice however a substantial density *of opposite sign* close to the bond axis, illustrating that the effect of σ–π mixing is to reduce the overall intensity of the $\pi \rightarrow \pi^*$ excitation.[65,23] The remaining two plots in Figure 7 contain contours in planes parallel to the *YZ* plane passing through C_2 for $\pi \rightarrow \pi^*$ and through the midpoint of C_2–H for $\sigma_y \rightarrow \pi^*$, respectively. Both of these plots show the dissymmetry in the transition density due to the rest of the molecule; for the $\sigma_y \rightarrow \pi^*$ excitation, the contours show the predominant quadrupolar character of the transition density, with dipole components introduced by the symmetry lowering and the saturated part of the ring. Figure 8 contains charge rearrangement density contours (eq 13) for the same excitations. In the case of the $\pi \rightarrow \pi^*$ excitation, the plots show rearrangement of charge from inner to outer regions in the process, whereas the plot of $\sigma_y \rightarrow \pi^*$ shows not only charge flow from the *XY* to the *XZ* plane, but also the substantial participation of the rest of the ring. Figures 7 and 8 clearly display quite different representations of these excitations, although some features, e.g., the σ–π mixing in the $\pi \rightarrow \pi^*$ transition, are apparent in both representations.

Turning now to the intensity of the various transitions in TCO and its fragments, we note the following trends in Table V. First, in all three fragments, the $\pi \rightarrow \pi^*$ transition shows considerable oscillator strength, and the rotatory strengths of the $\pi \rightarrow 3s$ and $\sigma_y \rightarrow \pi^*$ transitions retain their respective negative and positive signs, in accord with the observed spectrum of TCO. Beyond that, one finds little regularity in associating the computed intensities of the fragments with those of TCO itself. However, the main irregularities in correlating the rotatory intensities are associated with the $\pi \rightarrow 3d_{xy}$ transition and with the group of $\pi \rightarrow 3p_\perp$, $3p_\parallel$, and π^* transitions. Of these, the $\pi \rightarrow 3d_{xz}$ transition has an unexpectedly large rotatory strength in TCO-E, where it is close in energy to the $\sigma_y \rightarrow \pi^*$ transition, whereas its rotatory intensity is reduced considerably in TCO-B and TCO where this energy difference is much greater. For the threesome of excitations, $\pi \rightarrow \pi^*$, $\pi \rightarrow 3p_\perp$, and $\pi \rightarrow 3p_\parallel$, the intensity redistribution between the $\pi \rightarrow 3p_\perp$ and $\pi \rightarrow 3p_\parallel$ transitions is qualitatively understandable in view of the increasing requantization of these excitations in the sequence TCO-E, TCO-B, and TCO (see above). For the $\pi \rightarrow \pi^*$ mixing in particular, we notice that the symmetry lowering going from planar *trans*-2-butene to TCO-B allows considerable mixing between the $3p_\parallel$ and π^* IVO's. The result is that the 6.92-eV and the 7.22-eV transitions in TCO-B (basis B) can be designated as $\pi \rightarrow 3p_\parallel$ and $\pi \rightarrow \pi^*$, respectively, based upon their IVO contours. However, the weight of the $\pi \rightarrow \pi^*$ configuration in the 6.92-eV transition is only about twice as large as it is in the higher-lying one, and while it carries the largest oscillator strength, the 7.22-eV transition carries the entire rotatory strength. In TCO, this mixing persists, and our assignment of the third excitation as $\pi \rightarrow \pi^*$ and the fourth as $\pi \rightarrow 3p_\parallel$ is therefore based on the IVO plots rather than on charge rearrangements or weights of configurations in the normalizations. In fact, Figure 3 suggests that our basis B results tend to overestimate the $\pi \rightarrow \pi^*$ transition energy in TCO and hence its mixing with the less basis set-dependent $\pi \rightarrow 3p_\parallel$ excitation. The oscillator strength decompositions, eq 27, are dominated by a single term, $f^q_{\pi\pi}$, for all excitations out of the π orbital and are thus not displayed separately. Other couplings within the double bond reduce the overall intensity, in accord with the interpretation of Figure 7a, and the reduction of the $\pi \rightarrow \pi^*$ intensity going from ethylene to TCO is primarily due to a local effect on $f_{\pi\pi}$, rather than on couplings with the rest of the molecule. The ordinary intensity of the $\sigma_y \rightarrow \pi^*$ excitation arises from a combination of nearly canceling couplings within the σ bonds associated with C_3 and C_4.

Table V also contains the decomposition of the total rotatory strengths of TCO into terms representing the entire intrinsic, μ–m and μ–μ contributions (i.e., sums over all contributions according to eq 32, 33, and 34, respectively). In all cases, the intrinsic contribution from the bonding π orbital alone accounts for the entire intrinsic contribution to within $\pm 1 \times 10^{-40}$ cgs. It is clear from the table that all three Kirkwood mechanisms are operative for these transitions, even for the $\pi \rightarrow \pi^*$ and $\sigma_y \rightarrow \pi^*$ transitions which in zeroth order would be thought of as inherently dissymmetric (i.e., intrinsic dominated) electric and magnetic dipole-type excitations, respectively. This explicit calculation of the contributions from all the Kirkwood mechanisms therefore confirms the Scott and Yeh demonstration[15] of the importance of the polarizability contribution for this molecule.

To further analyze these intensity mechanisms, Table VI shows to what extent the contributions from the localized MO's in TCO mimic those from the corresponding localized orbitals in the TCO-E and TCO-B fragments. In the table, this comparison is

Table VI. Comparison of Rotatory Strength Contributions in TCO and Fragments (in Units of 10^{-40} cgs)

	chromophore[a]			butene-rest[b]		TCO-rest[c]
	1[d]	2	3	4	5	6
excitation[f]	TCO-E[e]	TCO-B	TCO	TCO-B	TCO	TCO
$\pi \rightarrow 3p_\perp$	−2	1	−6	5	−2	2
$\pi \rightarrow 3s$	−35	−13	−5	8	−2	2
$\pi \rightarrow \pi^*$	−114	−22	−46	21	1	−7
$\pi \rightarrow 3p_\parallel$	1	−46	3	−33	20	8
$\pi \rightarrow 3d_{xz}$	80	0	−15	4	−7	10
$\sigma_y \rightarrow \pi^*$	71	89	71	−25	−9	−15

[a] Contributions from C=C bonds and σ bonds corresponding to ethylene. Numbers in parentheses are the contributions from the π orbital alone. [b] σ bonds between atom pairs (3–5), (3–11), (3–12), (4–6), (4–13), and (4–14); see Figure 2. [c] σ bonds involving C_5, C_6, C_7, C_8, and attached hydrogens. [d] Columns numbered for easy reference in text. [e] Molecule from which bond set contributions are extracted; columns 3, 5, and 6 sum to the total TCO results. [f] Ordered and indexed corresponding to TCO.

Table VII. Computed Excitation Energies and Intensities for Equatorial and Axial Conformers of MCP

	MCP-E						MCP-A					
			$R^{\nabla}(10^{-40}$ cgs)						$R^{\nabla}(10^{-40}$ cgs)			
a	ΔE, eV	$f^{r\nabla}$	tot	intrins[b]	μ-m[c]	μ-μ[d]	ΔE, eV	$f^{r\nabla}$	tot	intrins[b]	μ-m[c]	μ-μ[d]
$\pi \rightarrow 3s$	6.48	0.02	-4	-1	-1	-2	6.53	0.03	-4	-1	-1	-2
$\pi \rightarrow 3p_z$	7.06	0.03	-1	-1	0	0	7.13	0.01	6	1	0	5
$\pi \rightarrow 3p_x$	7.20	0.01	-3	0	0	-3	7.26	0.00	-2	0	0	-2
$\pi \rightarrow \pi^*$	7.31	0.28	37	2	4	31	7.20	0.24	28	-10	10	28
$\pi \rightarrow 3p_y$	7.41	0.00	0	3	-3	0	7.47	0.03	29	11	-3	21
$\pi \rightarrow 3d_\sigma$	7.88	0.01	5	1	0	4	7.94	0.01	5	2	0	3
$\pi \rightarrow 3d_{xy}$	7.92	0.02	1	0	0	1	7.92	0.01	2	0	1	1
$\pi \rightarrow 3d_{xz}$	8.10	0.02	-8	-1	1	-8	8.17	0.03	-12	0	-1	-11
$\pi \rightarrow 4p_x$	8.60	0.00	1	-1	1	1	8.66	0.00	1	-1	1	1

[a] IVO assignments. [b] Total contributions from eq 32. [c] Total contributions from eq 33. [d] Total contributions from eq 34.

organized into three groups of bonds: (a) the "chromophore", consisting of the σ- and π-bond set corresponding to ethylene; (b) "butene-rest", the bonds (3–5), (3–11), (3–12), (4–6), (4–13), and (4–14); and (c) "TCO-rest", the remaining bonds involving C_5–C_8 and attached hydrogens. Inspection of the three chromophore columns shows how extensively these local contributions are influenced by the rest of the molecule through modification of the localized orbitals and changes in the nature and density of the virtual space. For the $\pi \rightarrow \pi^*$ transition, the correct sign is retained in the local contribution in all three molecules; however, as shown in parentheses, the π-orbital contribution alone has the wrong sign in the two fragments. Note that the methyl group contributions to the $\pi \rightarrow \pi^*$ and $\pi \rightarrow 3p_\parallel$ excitations in TCO-B (set 4) are large and oppositely signed, thus effectively transferring intensity from the former to the latter in accord with the discussion above. These methyl groups also cause an appreciable reduction in rotatory strength of $\sigma_y \rightarrow \pi^*$ in TCO-B and somewhat less so in TCO. The direct effect of the rest of the ring is shown in the last column of Table VI. These contributions become more important at higher energies; they are positive for the Rydberg excitations and negative for the valence excitations shown. However, apart from the $\sigma_y \rightarrow \pi^*$ transition, the direct effect of the rest of the ring is significantly less important than the indirect effects exhibited in the modification of the local chromophore and "butene-rest" contributions.

Finally, our results for TCO show the same structure as the experimental CD spectrum of Mason and Schnepp,[3] in which the first feature, from the long-wavelength side, is a weakly negative band[66] appearing as a shoulder on the intense negative band commonly assigned to $\pi \rightarrow \pi^*$. (We have estimated the experimental oscillator strength of the corresponding UV band to be about 0.15.[23]) Then the spectrum shows some structure with a weak CD signal, followed by an intense, positive band at higher energy. Figure 3 and Table V show the same clustering of excitations, beginning with the $\pi \rightarrow 3s$ and $\pi \rightarrow 3p$ group. The intense negative band is calculated to comprise both the $\pi \rightarrow \pi^*$ and the remaining $\pi \rightarrow 3p$ transitions, while the structure at higher energies is plausibly associated with the $\pi \rightarrow 3d$ and the lowest $\pi \rightarrow 4p$ excitations. The second intense band is the $\sigma_y \rightarrow \pi^*$ transition. Figure 9a shows a simulated CD spectrum for TCO, obtained by using the computed energies and intensities, and reasonable assumptions about half-widths, to generate a set of overlapping Gaussians. This simulated CD spectrum is shifted to higher energies by about 1 eV relative to the experimental spectrum, and it appears that the intensities of the Rydberg excitations are overestimated at the expense of the valence excitations. The latter feature corroborates the above-mentioned overestimate of the Rydberg/π^* mixing, and if we arbitrarily lower the Rydberg intensities by half, we obtain Figure 9b, which matches the observed spectrum quite well in both signs and magnitudes. For the number of states accounted for and the size of the molecule in an ab initio context, this is quite a satisfactory overall agreement. In view of the improved agreement with basis A in planar monoolefins, we believe that the present problem of overestimating the transition energies and of the Rydberg–valence intensity balance reflects basis set incompleteness rather than inherent limitations in the RPA method.[67]

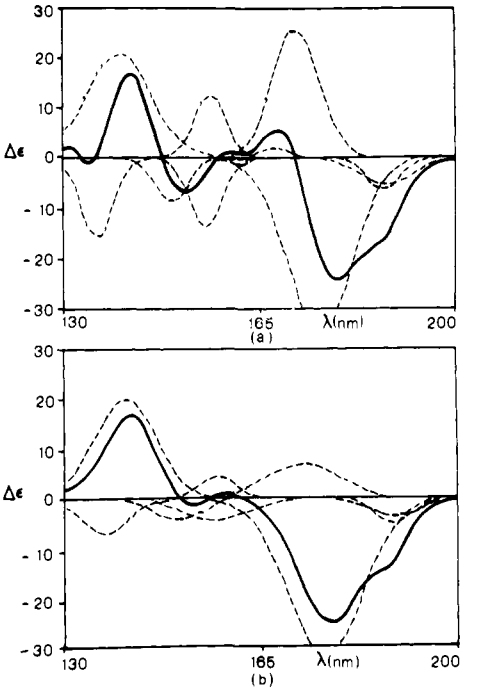

Figure 9. Simulated CD spectrum of TCO: (a) computed results used directly; (b) Rydberg intensities reduced by half. Half-widths for Gaussians vary from 4 to 10 nm.

VI. Methylcyclopentene

The computed SCF energies in Table III for the equatorial (MCPE) and axial (MCPA) conformer of MCP make the equatorial form about 2.2 kcal more stable than the axial form. Application of a second-order Møller-Plesset (MP2) correction[68] tips the balance the other way, favoring the axial form by 1.0 kcal, and the MM2 force field optimizations yield an energy difference of only about 0.2 kcal. Since the question of conformational preference therefore cannot be resolved by these calculations, we shall assume a 1:1 mixture of the two conformers in making comparisons to the experimental spectrum.[20]

The overall RPA results for MCPE and MCPA are shown in Table VII. Although only $f^{r\nabla}$ and R^{∇} are given, the other forms of the intensities were also computed and they agree with each other within 20% for the oscillator strengths and 10% for the rotatory strengths. As can be seen from Figure 4 and Table VII, the excitations for both MCPE and MCPA are grouped into four regions: (I) the $\pi \rightarrow 3s$ transition around 6.5 eV.; (II) the $\pi \rightarrow \pi^*$ and $\pi \rightarrow 3p$ manifold between 7.0 and 7.5 eV; (III) several $\pi \rightarrow 3d$ transitions grouped around 8 eV; and (IV) the $\pi \rightarrow 4p$ and other excitations beyond 8.5 eV, including presumably the $\sigma_y \rightarrow \pi^*$-type excitation which plays an important role in TCO, but which is not found among the lowest 18 transitions, covering energies up to about 9.2 eV. (A calculation using an unsplit diffuse orbital basis locates this excitation at 9.5 eV with a rotatory strength of only -5×10^{-40} cgs.) The energies of the $\pi \rightarrow$ Rydberg excitations show a uniform blue shift of ca. 0.05 eV going from

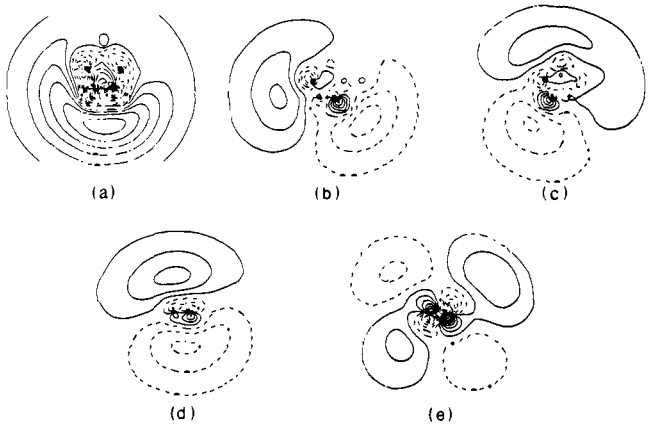

Figure 10. Contour plots of IVO's for MCPE: (a) 3s (*XY* plane); (b) $3p_x$ (*XY* plane); (c) $3p_y$ (*XY* plane); (d) $3p_z$ (*XZ* plane); (e) $3d_{xz}$ (*XZ* plane).

Table VIII. Association of Computed Excitations with Observed Bands in MCP, Assuming a 1:1 Mixture of MCPE + MCPA

	present			Levi et al.[a]			exptl.[a]	
band	assign	*f*	*R*	assign	*f*	*R*	*f*	*R*
I	$\pi \rightarrow 3s$	0.02	−4	$\pi \rightarrow 3s$ $\sigma \rightarrow 3s$	0.02	−8	0.03	−16
IIa	$\pi \rightarrow 3p_x$ $\pi \rightarrow 3p_z$ $\pi \rightarrow \pi^*$	0.28	+33	$\pi \rightarrow \pi^*$	0.50	+3	0.16	+26
IIb	$\pi \rightarrow 3p_y$	0.01	+15	$\pi \rightarrow 3p_x$ $\sigma \rightarrow 3p_x$		+4	shoulder	shoulder
III	$\pi \rightarrow 3d$	0.05	−4	$\pi \rightarrow 3p_y$ $\pi \rightarrow 3p_z$	0.01	−6	0.09	−16

[a] Reference 20.

MCPE to MCPA, while the $\pi \rightarrow \pi^*$ transition red-shifts by 0.1 eV, perhaps due to enhanced delocalization ("hyperconjugation") onto the axial methyl group. Because of strong configurational mixing in the RPA eigenvectors, we again base our assignments on IVO contour plots. Figure 10 shows IVO plots for the 3s, $3p_x$, $3p_y$, $3p_z$, and $3d_{xz}$ upper orbitals; the last of these in particular could not be pictured from an examination of the various numerical coefficients. The 3s and 3p IVO's show distortion caused by the methyl group but are otherwise clearly identifiable.

The various intensities in Table VII are comparable between the conformers, with the exception of the $\pi \rightarrow 3p_y$ excitation at the blue end of region 2. The rotatory strength of this transition is negligible in MCPE but is comparable to that of the strong $\pi \rightarrow \pi^*$ band in MCPA. In Table VIII, we collect our computed results into bands corresponding to the observed spectrum and compare them with experiment and with the calculations of Levi et al.,[20] and Figure 11 shows a simulation of the CD spectrum based on Table VII, again assuming a 1:1 mixture of the two conformers. While the figure suggests some imbalance between Rydberg and valence excitations, the overall agreement with the experimental CD spectrum[20] is quite satisfactory, both in regard to magnitudes and sign distribution. We agree with Levi et al.[20] on the location and sign of the $\pi \rightarrow \pi^*$ transition (however, their $\pi \rightarrow \pi^*$ rotatory strength is low by almost an order of magnitude) but differ with them on several other assignments. Most notably, we find no evidence for low-lying excitations out of σ orbitals, in contrast to their suggested $\sigma \rightarrow 3s$ and $\sigma \rightarrow 3p_x$ contribution to band I and IIb. In addition, we assign the asymmetric tail on the blue side of the $\pi \rightarrow \pi^*$ transition to the $\pi \rightarrow 3p_y$ excitation of the axial conformer, whereas Levi et al.,[20] who use a geometry that does not distinguish between conformers, assign this shoulder to a mixture of $\pi \rightarrow 3p_x$ and $\sigma \rightarrow 3p_x$ (our notation). Finally, although band III is assigned by the two approaches as $\pi \rightarrow 3d$ and $\pi \rightarrow 3p$, respectively, both calculations yield rotatory strengths of correct sign and magnitude for this band. Apart from the fact that the geometry used in ref 20 is not optimized, the consistent picture of monoolefin spectra that emerges from the present

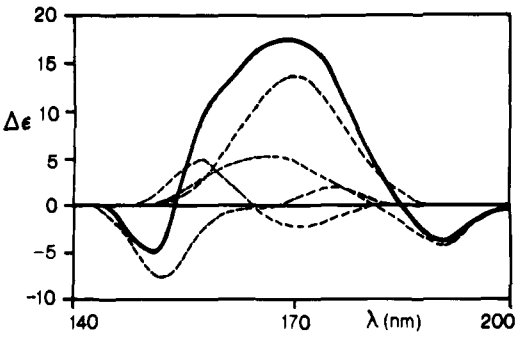

Figure 11. Simulated CD spectrum of MCP, assuming 1:1 mixture of MCPE and MCPA. Half-widths vary from 5 to 11 nm.

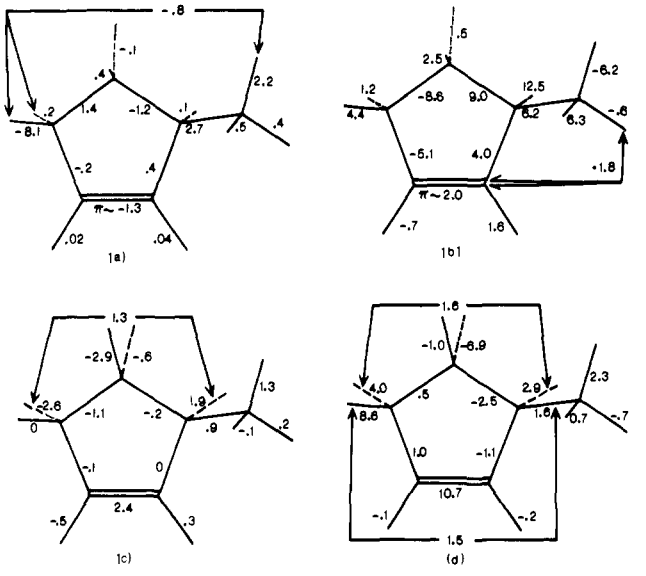

Figure 12. Bond couplings $R_{\pi\beta}$, with π orbital in MCP: (a) $\pi \rightarrow 3s$ (MCPE), total $R^{\nabla} = -3.6$ ($\times 10^{-40}$ cgs), $\sum_\beta R_{\pi\beta} = -2.5$; (b) $\pi \rightarrow \pi^*$ (MCPE), total $R^{\nabla} = 36.8$, $\sum_\beta R_{\pi\beta} = 29.1$; (c) $\pi \rightarrow 3p_y$ (MCPE), total $R^{\nabla} = -0.4$, $\sum_\beta R_{\pi\beta} = -0.9$; (d) $\pi \rightarrow 3p_y$ (MCPA), total $R^{\nabla} = 28.8$, $\sum_\beta R_{\pi\beta} = 19.9$.

calculations lends weight to our assignments over those of Levi et al. for MCP.

Table VII also shows the contribution of the intensity mechanisms (eq 32–34) to the overall rotatory strengths, and again all three mechanisms contribute for most of the excitations, although the polarizability or μ–μ coupling tends to dominate. As it turns out, for the important lowest excitations, namely $\pi \rightarrow 3s$, $\pi \rightarrow \pi^*$, and $\pi \rightarrow 3p_y$, most of the important coupling terms $R_{\alpha\beta}$ (eq 31) involve the bonding π-orbital; hence the contributions can be readily displayed on a diagram of the molecule. Figure 12a shows the terms $R_{\pi\beta}$ for each bond in the $\pi \rightarrow 3s$ excitation of MCPE. Contributions from the ring C–C bonds are roughly antisymmetric across the y–z plane, and the α-equatorial bonds also show a sign change. The most distinctive feature for this excitation is the enhancement shown by the extended bond path C_2–C_3–C_6–H_{16} and C_1–C_5–H_{12}. This enehancement is reminiscent of that shown by the bond zigzag extending from the C=O group in ketones.[45] The $R_{\pi\beta}$ terms account for 70% of the total rotatory strength; $R(\mu,\mu)$ terms account for 64% of the $R_{\pi\beta}$ sum. Figure 12b shows the $R_{\pi\beta}$ terms for the $\pi \rightarrow \pi^*$ excitation in MCPE. Once again, the ring bond contributions change sign across the yz plane, but now the out-of-plane bond terms do not. The quasi-axial C_3–H_9 bond exerts the largest single coupling, and the other quasi-axial bonds show couplings several times larger than in $\pi \rightarrow 3s$. Of particular interest here is the quite different distribution of methyl C–H coupling terms, relative to those in $\pi \rightarrow 3s$.

Finally, Figure 12c and d compares the $R_{\pi\beta}$ terms for the $\pi \rightarrow 3p_y$ transition in MCPE and MCPA, respectively. In this

excitation, the intrinsic term $R_{\pi\pi}$ is much larger for MCPA than for MCPE; the interpretation is that the methyl group exerts a stronger perturbation on the π orbital in the axial form than in the equatorial form, whereas the methyl group itself plays little role in the bond–bond couplings. The bond–bond couplings between the allylic bonds and the π orbital are again stronger for the axial than for the equatorial bonds, and the back axial C–H bond (C_4–H_{11} in MCPE, C_4–H_{10} in MCPA) contributes quite strongly in this excitation, despite the fact that it is located in a symmetry plane of the ethylenic chromophore. Cross-ring couplings between pairs of corresponding allylic bonds are also significant in this excitation. The large R value for this excitation in MCPA therefore appears to be due primarily to the interactions of the allylic axial bonds with the π orbital, both by intrinsic and by μ–μ coupling mechanisms.

VII. Concluding Remarks

For molecules of the size considered here, simple orbital promotion pictures for the assignment and description of the excitations break down. We have demonstrated the application of a variety of techniques for the analysis of computed excitation properties. These techniques range from contour plots of transition and rearrangement densities and of improved virtual orbitals, over computer simulations of the spectra, to bond decompositions of the intensities, including subdivisions of these bond contributions into "mechanisms". The mechanisms are based on Kirkwood's theory of optical activity,[33,34] and it is an important feature of our approach that these mechanistic bond contributions involve no approximations beyond those entering the overall scheme used for computing the electronic excitation properties. For the present set of molecules, we find that the random phase approximation in moderately extended basis sets provides transition energies and total intensities of a quality that warrants such close scrutiny.[71]

The two molecules of primary interest here, (−)-*trans*-cyclooctene and (3*R*)-3-methylcyclopentene, both contain an ethylenic chromophore, and the resulting spectra can be discussed in terms borrowed from ethylene assignments. However, the various contour plots and correlation diagrams show that orbital distortions and energy reorderings, induced by the lowering of local symmetry and participation of the rest of the molecules, produce excitations that are qualitatively different from those of ethylene. A particularly striking illustration is provided by two of the 3p Rydberg excitations in *trans*-cyclooctene which become quantized relative to the gross structure of the molecule, rather than relative to the chromophore symmetry axes. The use of spectrum simulations for comparisons with experiments is almost mandatory, because of the high density of excitations and the intricate sign variations of the rotatory strengths. The present spectrum simulations should not be taken too literally of course, since the resulting band shapes can be varied markedly by variations in the widths chosen for the individual contributions. However, the semiquantitative agreements with the experiments, over a range covering up to ten individual excitations, strongly support our assignments and overall intensity signs and magnitudes.

As for the intensity mechanisms, our analyses show that neither of the two molecules can be described adequately by only one coupling type, although the μ–μ or polarizability contributions generally agree in sign and order of magnitude with the total rotatory intensities. It should be noted that the present polarizability terms, eq 34, contain excitation-specific bond transition moments, eq 23–25; we have not attempted to extract general bond polarizabilities that could be used to construct the molecular optical properties in the sense of conventional polarizability theories.[58] For the individual transitions, we find that the rotatory strengths of the $\pi \rightarrow 3s$ and $\pi \rightarrow \pi^*$ transitions depend upon quite different structural features. Hence, there seems to be no reliable correlation between the CD signs of these two excitations in a series of molecules, and since these monoolefins, moreover, show a number of other Rydberg excitations in the same spectral range, attempts to make structural assignments based on assumed $\pi \rightarrow 3s$ and $\pi \rightarrow \pi^*$ rotatory strengths are a risky business. Drake and Mason,[9] in an analysis of the CD spectra of chiral olefins, propose an "olefin CD couplet" consisting of an essentially equal admixture of "$\pi \rightarrow \pi^*$" and "$\pi \rightarrow \pi_y$" (the ethylene $\pi \rightarrow 3p_y$ in our notation) transitions. We agree with them on the near-degeneracy of these two bands, and we do find evidence of substantial intensity borrowing. But our calculations indicate that this mixing does not necessarily lead to an oppositely signed pair of CD bands; moreover, the observed pair of strong, oppositely signed bonds in *trans*-cyclooctene and methylcyclopentene are not due to the same pair of excitations. In fact, the $\sigma_y \rightarrow \pi^*$ excitation which is the high-energy component in the *trans*-cyclooctene couplet apparently plays no role in the CD spectrum of methylcyclopentene.

The clear connection to ground-state molecular structural features afforded by the bond decompositions in eq 27 and 32–34 arises from the introduction of localized occupied orbitals and local magnetic moments. From these features and the characteristics of the random-phase approximation, we have also derived a local-origin variant of the coupled Hartree–Fock method for NMR shieldings that can be similarly analyzed in structural terms. This method, together with ^{13}C results for a number of organic molecules, is presented elsewhere.[62a]

Acknowledgment. We are grateful to the National Science Foundation (Grant CHE-82-18216), the NATO Scientific Affairs Division (Grant RG138.81), and the Danish Natural Sciences Research Council (Grant 11-3547) for support of this work. We also thank Dr. Nelson Beebe for a copy of the PLOT 76 graphics package that was used for the contour plots.

Appendix. Population Analysis of Transition and Rearrangement Densities

Let

$$\phi_i = \sum_s \chi_s C_{si} \tag{A1}$$

be the atomic orbital expansion of molecular orbital ϕ_i. The transition density (eq 11) can then be written

$$\rho_{0,q}(\mathbf{r}) = \sum_s \sum_t \chi^*_s(\mathbf{r}) \chi_t(\mathbf{r}) D_{st}^q \tag{A2}$$

where

$$D_{st}^q = \sum_\alpha \sum_m C_{s\alpha}(X_{\alpha m,q} + Y_{\alpha m,q}) C_{tm} \tag{A3}$$

determines the expansion into atomic orbitals. A population analysis of eq A2 is obtainable by use of the Mulliken approximation

$$\chi^*_s(\mathbf{r})\chi_t(\mathbf{r}) = \tfrac{1}{2} S_{st}\{\chi_s^2(\mathbf{r}) + \chi_t^2(\mathbf{r})\} \tag{A4}$$

where $S_{st} = \langle \chi_s | \chi_t \rangle$ is the overlap integral. Equations A2–A4 yield

$$\rho_{0,q}(\mathbf{r}) = \sum_s \chi^2_s(\mathbf{r}) \lambda_{s,q} \tag{A5}$$

where

$$\lambda_{s,q} = D_{ss}^q + \tfrac{1}{2} \sum_{t \neq s} S_{st}(D_{st}^q + D_{ts}^q) \tag{A6}$$

is the gross transition population in orbital s for this excitation. Summing eq A6 over all orbitals on an atom A produces the gross atomic transition population

$$\Lambda_{A,q} = \sum_s \lambda_{s,q} \tag{A7}$$

Notice that eq 10 implies that

$$\sum_s \lambda_{s,q} = \sum_A \Lambda_{A,q} = 0 \tag{A8}$$

Analogously, the rearrangement density (eq 13) has the atomic orbital expansion

(71) The RPA includes only first-order electron correlation effects on the excitation, and the use of the Hartree–Fock ground state is an additional inherent approximation; our results on planar monoolefins,[62b] however, appear to indicate that truncation of the atomic basis set for the large molecules treated here is at least as significant a source of error.

$$\Delta_{0,q}(\mathbf{r}) = \sum_s \sum_t \chi^*_s(\mathbf{r})\chi_t(\mathbf{r})P_{st}^q \quad \text{(A9)}$$

with

$$P_{st}^q = \sum_{\alpha m} \sum_{\beta n} \{C_{sm}C_{tn}\delta_{\alpha\beta} - C_{s\alpha}C_{t\beta}\delta_{mn}\}\Xi_{\alpha m,\beta n}^q \quad \text{(A10)}$$

Use of the Mulliken approximation (eq A4) yields the population analysis expression

$$\Delta_{0,q}(\mathbf{r}) = \sum_s \chi_s^2(\mathbf{r})\gamma_{s,q} \quad \text{(A11)}$$

where

$$\gamma_{s,q} = P_{ss}^q + \sum_{t \neq s} S_{st}P_{st}^q \quad \text{(A12)}$$

is the rearrangement population in orbital s. The gross atomic rearrangement population on atom A is obtained by summing eq A13 over all orbitals on A, i.e.,

$$\Gamma_{A,q} = \sum_s^A \gamma_{s,q} \quad \text{(A13)}$$

It follows from eq 16 that

$$\sum_s \gamma_{s,q} = \sum_A \Gamma_{A,q} = 0 \quad \text{(A14)}$$

Computationally, the orbital populations (eq A6 and A13) provide useful information about which parts of the atomic orbital basis are particularly involved in a given set of excitations, and they can hence guide the search for optimal basis sets. Moreover, since they incorporate the entire sum over configurations $\alpha \rightarrow m$, they can often clarify the nature of the excitation and of possible IVO descriptions.

Note Added in Proof. After this paper was accepted, a theoretical study appeared of the CD spectrum of (3*R*)-3-methylcyclobutene (MCB),[72] resulting in spectral assignments that differ from those originally proposed.[73] Since the chiroptical properties of MCB fit naturally into the present context, we have calculated them in our basis B, using the MINDO-optimized geometry of ref 72. The resulting RPA calculations encompassed 728 particle–hole excitations.

Our results for the lowest five excitations are as follows: ΔE = 6.70 eV ($\pi \rightarrow 3s$), $f^{r\nabla}$ = 0.029, R^{∇} = −2.3; ΔE = 7.09 eV ($\pi \rightarrow \pi^*$), $f^{r\nabla}$ = 0.209, R^{∇} = −30.9; ΔE = 7.25 eV ($\pi \rightarrow 3p$), $f^{r\nabla}$ = 0.017, R^{∇} = 6.7; ΔE = 7.31 eV ($\pi \rightarrow 3p$), $f^{r\nabla}$ = 0.020, R^{∇} = 12.1; ΔE = 7.25 eV ($\pi \rightarrow 3p$), $f^{r\nabla}$ = 0.14, R^{∇} = 16.9 In addition, ring strain destabilizes the σ orbitals, so that the $\sigma_y \rightarrow \pi^*$ excitation (no. 9) drops down to 8.48 eV (R^{∇} = 12.6) in MCB. Another valence excitation, $\sigma_{CC} \rightarrow \pi^*$, is computed to lie at 9.20 eV, as the twelfth excitation.

MCB shows a strong negative CD band at 6.49 eV, with $\Delta\epsilon$ = −10.4 (corrected to 100% optical purity), and a shoulder at 6.42 eV with $\Delta\epsilon$ = −7.6. These features were assigned as $\pi \rightarrow \pi^*$ and $\pi \rightarrow 3s$, respectively.[73] In ref 72, however, a *positive* $\pi \rightarrow \pi^*$ rotatory strength was obtained in a variety of basis sets. Their largest calculation ("DZD") placed the $\pi \rightarrow 3s$ at 7.14 eV with f_{av} = 0.012 and R_{av} = −3.65, and $\pi \rightarrow \pi^*$ as the third excitation at 8.18 eV with f_{av} = 0.037 and R_{av} = +3.4. The present calculations are thus consistent with the experimental data and original assignments[73] but differ markedly from the calculations recently reported.[72]

Registry No. (3*R*)-3-Methylcyclopentene, 39750-38-4; (−)-*trans*-cyclooctene, 931-89-5.

(72) Chabalowski, C. F.; Maggiora, G. M.; Christoffersen, R. E. *J. Am. Chem. Soc.* **1985**, *107*, 1632.
(73) Rossi, R.; Diversi, P. *Tetrahedron* **1970**, *26*, 5033.

Stable Hydrogen-Bonded Isomers of Covalent Ions. Association of Carbonium Ions with n-Donors

Michael Meot-Ner (Mautner),*† Mark M. Ross,‡ and Joseph E. Campana‡

Contribution from the Chemical Kinetics Division, Center for Chemical Physics, National Bureau of Standards, Gaithersburg, Maryland 20899, and the Naval Research Laboratory, Chemistry Division, Washington, D.C. 20375-5000. *Received February 12, 1985*

Abstract: Addition reactions of carbonium ions R^+ with n-donors such as H_2O can produce covalent condensation products ROH_2^+, or cluster adducts $H_2O\cdots R^+$. While $\Delta S°_{condensation}$ is −35 to −40 cal mol^{-1} K^{-1}, the measured values for several reactions are only −20 to −24 cal mol^{-1} K^{-1}, which indicates cluster formation. A review of thermochemical data of 15 addition reactions suggests that in eight reactions a cluster involving $XH^+\cdots Y$ or $CH^{\delta+}\cdots X$ hydrogen bonding is favored over a covalent condensation product. This may result from enthalpy factors, or, when $\Delta H°$ for condensation and clustering is comparable, from the more favorable entropy of the loose cluster product. Such thermochemical factors apply to the addition of H_2O and CH_3OH to the oxocarbonium ions $CH_3CH^+OCH_3$ and $(CH_3)_2C^+OCH_3$, where the incipient covalent bond is weakened due to the stabilization of the ions. The adducts are cluster ions rather than protonated acetals and hemiacetals; nevertheless, limits on the $\Delta H_f°$ of the protonated acetals and hemiacetals, and on the proton affinities of these compounds, in the range of 202–207 kcal mol^{-1}, can be derived. In other addition reactions of carbonium ions, we find that the collisional dissociation spectra of the adducts of CH_3^+, $C_2H_5^+$, *i*-$C_3H_8^+$, and *t*-$C_4H_9^+$ with H_2O are identical with those of protonated alcohols and amines, except for *i*-$C_3H_7^+\cdot H_2O$ and *t*-$C_4H_9^+\cdot H_2O$, where another structure, presumably a cluster ion, is formed. These results are consistent with thermochemical predictions. The possibility of clustering must be considered in the thermochemical uses of association data, and in the contribution of ion–molecule association to atmospheric synthesis.

The formation and subsequent condensation of carbonium ions occurs in numerous organic reactions. In the gas phase, the association of carbonium ions with n-donors may contribute to organic synthesis in ionized atmospheres. Such reactions are, for example, the association of CH_3^+, $C_2H_5^+$, *sec*-$C_3H_7^+$, and *t*-$C_4H_9^+$ with H_2O,[1] NH_3 or alkylamines,[2] and HCN or CH_3CN.[3] The structures of the association products are of interest, because the empirical formulas of the products are identical with those of protonated alcohols, amines, and cyanides or isocyanides. For

† National Bureau of Standards.
‡ Naval Research Laboratory.

(1) Hiraoka, K.; Kebarle, P. *J. Am. Chem. Soc.* **1977**, *99*, 360.
(2) Meot-Ner (Mautner), M. *J. Am. Chem. Soc.* **1979**, *101*, 2389.